Accepted Manuscript

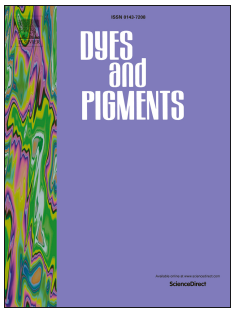

Synthesis of heteroleptic iridium complexes with sterically hindered methyl groups on pyrazole ligands for efficient yellow and green light-emitting electrochemical cells

Chozhidakath Damodharan Sunesh, Madayanad Suresh Subeesh, Kanagaraj Shanmugasundaram, Ramesh Kumar Chitumalla, Joonkyung Jang, Youngson Choe

PII: S0143-7208(16)30015-8

DOI: 10.1016/j.dyepig.2016.01.033

Reference: DYPI 5087

To appear in: *Dyes and Pigments*

Received Date: 27 November 2015

Revised Date: 13 January 2016

Accepted Date: 25 January 2016

Please cite this article as: Sunesh CD, Subeesh MS, Shanmugasundaram K, Chitumalla RK, Jang J, Choe Y, Synthesis of heteroleptic iridium complexes with sterically hindered methyl groups on pyrazole ligands for efficient yellow and green light-emitting electrochemical cells, *Dyes and Pigments* (2016), doi: 10.1016/j.dyepig.2016.01.033.

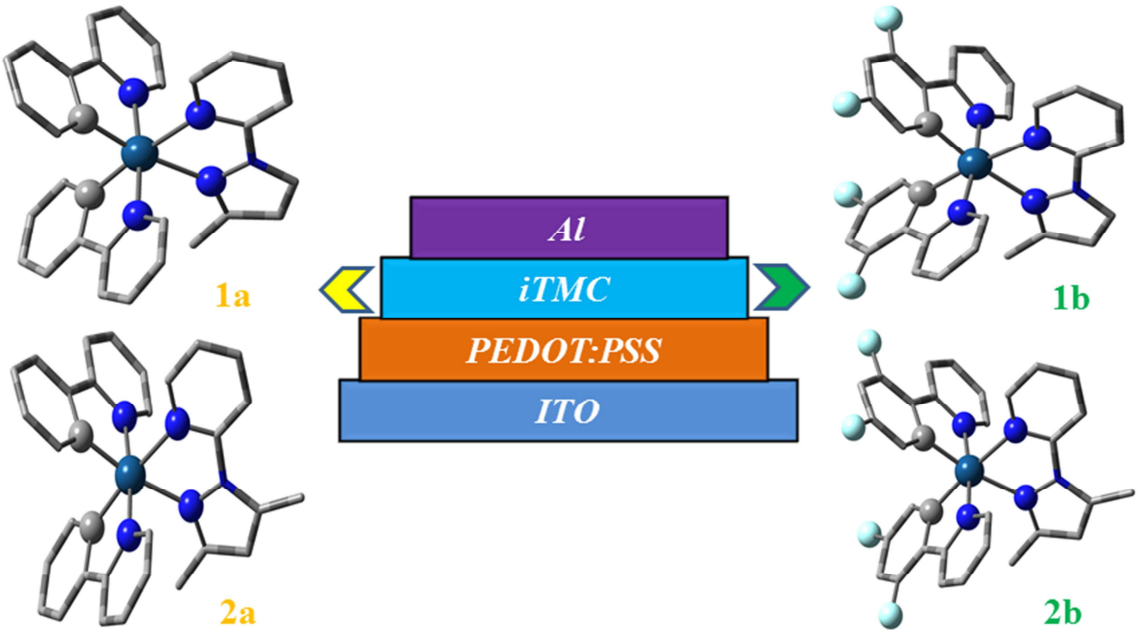

Synthesis of heteroleptic iridium complexes with sterically hindered methyl groups on pyrazole ligands for efficient yellow and green light-emitting electrochemical cells

Chozhidakath Damodharan Sunesh[a], Madayanad Suresh Subeesh[a], Kanagaraj Shanmugasundaram[a], Ramesh Kumar Chitumalla[b], Joonkyung Jang[b], and Youngson Choe[a]*

[a]Department of Polymer Science and Chemical Engineering,

Pusan NationalUniversity, Busan 609-735, South Korea

[b]Department of Nanoenergy Engineering,

Pusan National University, Busan, 609-735, Republic of Korea

*Corresponding author: *choe@pusan.ac.kr*

* Corresponding author. Tel.: +8251 510 2396; Fax: +8251 512 8634

KEYWORDS: Optical materials; Thin film; Vacuum deposition; Luminescence; Electrochemical properties

ABSTRACT: We report the synthesis of four cationic iridium complexes, $[Ir(ppy)_2(mepzpy)]PF_6$ (**1a**), $[Ir(dfppy)_2(mepzpy)]PF_6$ (**1b**), $[Ir(ppy)_2(dmpzpy)]PF_6$ (**2a**), and $[Ir(dfppy)_2(dmpzpy)]PF_6$ (**2b**), containing the methyl-substituted pyrazole-based ancillary ligand and the phenylpyridine-based cyclometalating ligands. UV–visible, photoluminescence (PL), and voltammetric measurements were made to study the photophysical and electrochemical properties of complexes **1a–2b**. Light-emitting electrochemical cells (LECs) were fabricated, which showed yellow emission for complexes **1a** and **2a** and green emission for complexes **1b** and **2b**. The LEC incorporating **2b** exhibited a high luminance of 658 cd m^{-2} and a current efficiency of 0.34 cd A^{-1}. The higher luminance and efficiency of the device based on **2b** were due to the smooth surface morphology and the presence of sterically hindered dimethyl groups on the ancillary ligand (dmpzpy), which causes a more balanced charge carrier injection and recombination.

1. Introduction

Light-emitting electrochemical cells (LECs) became prominent as a promising alternative to conventional organic light-emitting diodes (OLEDs) because of their simple device architecture, easy fabrication and low-cost production [1-5]. OLEDs are multilayered devices with a neutral emissive active layer and require air-sensitive low-work-function electrodes, in addition to the electron and hole injection layers. The resulting device necessitates rigorous encapsulation, which increases the production cost. Unlike OLEDs, LECs use an ionic active material, which makes them very simple and can be effortlessly processed from solution. Moreover, LECs independent of air-sensitive charge injection layers and metals, allowing nonrigorous encapsulation of the devices. These benefits make LECs a favorable candidate for next-generation display and lighting applications.

The first solid-state LEC device was introduced in 1995 and was based on a polymer blend, specifically, a mixture of an emissive conjugated polymer, an ion-conducting polymer, and an inorganic salt [1]. LECs with ionic transition metal complexes (iTMCs) were introduced there after [6-14]. The first iTMC-LEC, reported in 1996, was based on a ruthenium polypyridyl complex and emitted orange-red light with a maximum luminance of 30–50 cd m^{-2} under a forward bias [6]. Thereafter remarkable efforts have been made on LECs based on iTMCs to enhance the performance of the device. Consequently, iTMC-based LECs have exhibited increasing responsiveness owing to their phosphorescent nature. In comparison with polymer LECs, iTMC-LECs have a simpler device configuration, do not need an ion-conducting polymer or an inorganic salt for charge injection purposes, and possess high ionic conductivity. In addition, iTMCs are easily soluble in benign solvents, so these materials can be prepared by spin-coating on large-area devices. Furthermore, the light emission from iTMCs is from triplet

states, so they exhibit higher luminance efficiency and outstanding phosphorescent quantum yields compared to singlet emitters [3, 13, 15, 16]. Moreover, iTMCs display stable oxidation states and possess favorable excited state properties. The existence of these stable multiple redox states suggests that charge carriers can be easily injected and transported in these materials [17]. Under an applied bias, the mobile ions in the active layer of the LEC move toward the respective electrodes, creating an electrical double layer, which is followed by the injection of holes and electrons from the anode and cathode, respectively. These charge carriers move and combine to form excitons in which a fraction recombines radiatively, resulting the emission of light.

The representative iTMCs used in LEC devices are based on a ruthenium-(II)-containing complex as the single active component [6]. The low ligand-field splitting energies (LFSEs) of ruthenium(II) results the emission band of these ruthenium(II) complexes to be centered in the orange-red region of visible spectrum. The limited color tuning capability of these ruthenium complexes has thus restricted their application in lighting technologies [6-8, 18, 19]. Moreover, these complexes exhibit low stability under device conditions. The use of cyclometalated Ir(III) complexes in lighting devices offers remarkably improved device performance compared to the use of other metal complexes [5, 12, 20-26]. An LEC based on a cationic iridium complex, $[Ir(ppy)_2(dtb\text{-}bpy)]PF_6$ was reported for the first time by Slinker *et al.* in 2004 [3]. Single-layered LEC devices incorporating $[Ir(ppy)_2(dtb\text{-}bpy)]PF_6$ produced yellow light with a peak brightness and power efficiency of of 300 cdm^{-2} and 10 lm W^{-1}, respectively under 3 V [3]. Cationic iridium complexes are characterized by high spin–orbit coupling owing to their large size and charge. The high spin–orbit coupling leads to efficient intersystem crossing, resulting in high emission quantum efficiencies. Moreover, iridium complexes hold large LFSEs which leads the color tunning from blue to red through structural modification of cyclometalating and ancillary ligands.

In addition to the color tunability, these bis-cyclometalated iridium(III) complexes show excellent thermal and photochemical stability. However, during device operation, LECs based on these complexes experienced severe excited state self-quenching because the complexes in an active layer of LECs are closely packed. By incorporating adequate substituents on ancillary ligands through bulky groups or π–π interaction, it is possible to suppress these nonradiative pathways by creating an enlarged intermolecular distance and thereby to improve both the efficiency and the device lifetime [27-30]. We recently reported the synthesis of a series of cationic iridium complexes containing alkylated-benzimidazole-based ancillary ligands and studied the effect of the chain length on the electroluminescent properties [31]. LECs based on these alkylated-imidazole-based iridium complexes exhibited high efficiencies with increasing chain length from methyl to octyl groups due to the reduced intermolecular interactions and self-quenching [31].

Herein, we report the synthesis and characterization of four cationic iridium complexes with methyl-substituted pyrazole ligands, namely, $[Ir(ppy)_2(mepzpy)]PF_6$ (**1a**), $[Ir(dfppy)_2(mepzpy)]PF_6$ (**1b**), $[Ir(ppy)_2(dmpzpy)]PF_6$ (**2a**) and $[Ir(dfppy)_2(dmpzpy)]PF_6$ (**2b**), where mepzpy is 2-(3-methyl-1H-pyrazol-1-yl)pyridine, dmpzpy is 2-(3,5-dimethyl-1H-pyrazol-1-yl)pyridine, Hppy is 2-phenylpyridine, and Hdfppy is 2-(2,4-difluorophenyl)pyridine. The photoluminescence (PL) spectra of complexes **1a** and **2a** in acetonitrile solution show blue-green emission, whereas complexes **1b** and **2b** emit in the blue region of the visible spectrum. Density functional theory (DFT) and time-dependent DFT (TDDFT) calculations were performed for complexes **1a–2b**, and the obtained results are consistent with the experimental photophysical and electrochemical data. LECs were fabricated that produced yellow emission when complexes **1a** and **2a** were used and green emission when complexes **1b** and **2b** were used. Among the

complexes, LECs based on **2b** resulted the highest luminance, 658 cd m^{-2} and current efficiency, 0.34 cd A^{-1}, due to the reduced intermolecular interaction and self-quenching, which resulted in inhibition of the nonradiative pathways. In addition, complex **2b** showed smooth surface morphology, which again enhance the device performance by decreasing the charge transfer resistance at the interface of electrode.

Results and Discussion

Synthesis and characterization of heteroleptic iridium complexes (1a–2b)

The ancillary ligands (mepzpy and dmpzpy) were synthesized by a noncatalyzed C–N coupling reaction of 2-bromopyridine with 3-methyl-1H-pyrazole/3,5-dimethyl-1H-pyrazole in presence of potassium *tert*-butoxide [32]. The cationic iridium complexes were synthesized according to the previously reported procedures [33, 34]. First, commercially available $IrCl_3.xH_2O$ (1 equiv.) was treated with 2.2 equiv. of the corresponding cyclometalating ligands (C^N), namely, 2-phenylpyridine (Hppy) or 2-(2,4-difluorophenyl)pyridine (Hdfppy) in 2-ethoxyethanol and water (3:1, 40 mL) mixture to give a cyclometalated Ir^{III} μ-dichloro-bridged dimer, $[Ir(C^N)_2(\mu\text{-}Cl)]_2$. Next, heteroleptic cationic iridium complexes (**1a, 1b, 2a, and 2b**) were synthesized by reacting the desired dimeric complex with the preferred neutral ancillary ligands. The iridium complexes were formed as chloride salts and underwent anion metathesis reaction with solid NH_4PF_6 to replace Cl^-. The complexes obtained in high yields were characterized by elemental analysis, NMR and mass spectroscopic methods. The synthetic routes with the structures of ancillary ligands and cationic iridium complexes are shown in **Figure 1**.

Figure 1. The synthetic routes with the structures of ancillary ligands and cationic iridium complexes (**1a, 1b, 2a, and 2b**).

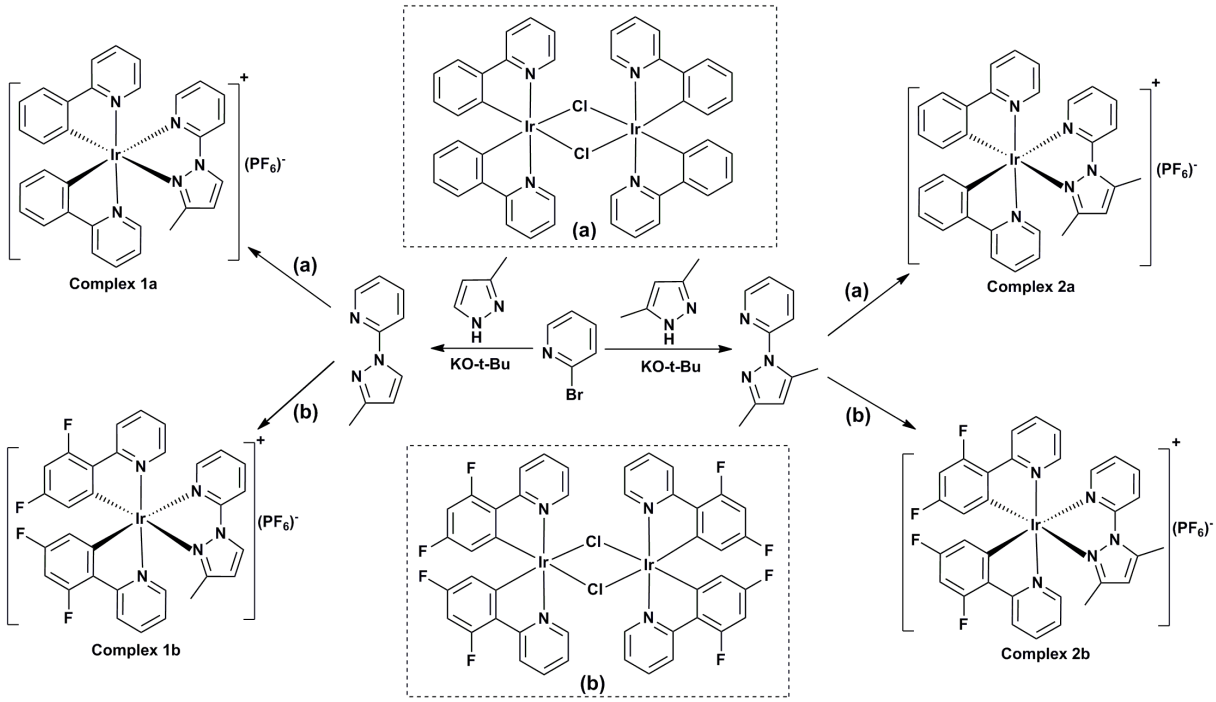

Photophysical properties

Figure 2 shows the room temperature UV–visible absorption spectra of the complexes in acetonitrile solution. All the complexes (**1a, 1b, 2a, and 2b**) show intense absorption bands ($\varepsilon > 2.5 \times 104\ M^{-1}\ cm^{-1}$) between 200 and 300 nm in the ultraviolet region. These high-energy bands are attributed to ligand-centered (LC) singlet $^1\pi\text{—}\pi^*$ transitions in both the coordinated cyclometalating and ancillary ligands. Following the LC bands, broad and less intense absorption bands are observed from 330 nm extending toward the visible region. These lower-energy bands are related to both spin-allowed and forbidden metal-to-ligand charge transfer (^{1}MLCT and ^{3}MLCT), ligand-to-ligand charge transfer (^{3}LLCT and ^{1}LLCT), and LC $^3\pi\text{—}\pi^*$ transitions of the complexes [35]. The considerable intensity of the spin-forbidden transitions (^{3}MLCT, ^{3}LLCT,

and ^{3}LC) is the result of strong spin–orbit coupling of the heavy iridium center, which facilitates the mixing of these states with higher-lying ^{1}MLCT transitions [34, 36]. The main absorption bands and molar extinction coefficients of all the complexes are given in **Table 1**. The absorption spectra in the lower-energy region of complexes **1b** and **2b** are significantly blue-shifted by 20 nm compared to those of complexes **1a** and **2a**. The hypsochromic shift in the absorption spectra is ascribed to the presence of electron─withdrawing fluorine atoms on the cyclometalated ligands of the complexes **1b** and **2b**. It is clear from **Figure 2** that alkyl substitution on ancillary ligands does not significantly affect the absorption spectra of the complexes, unlike the change in cyclometalating ligands.

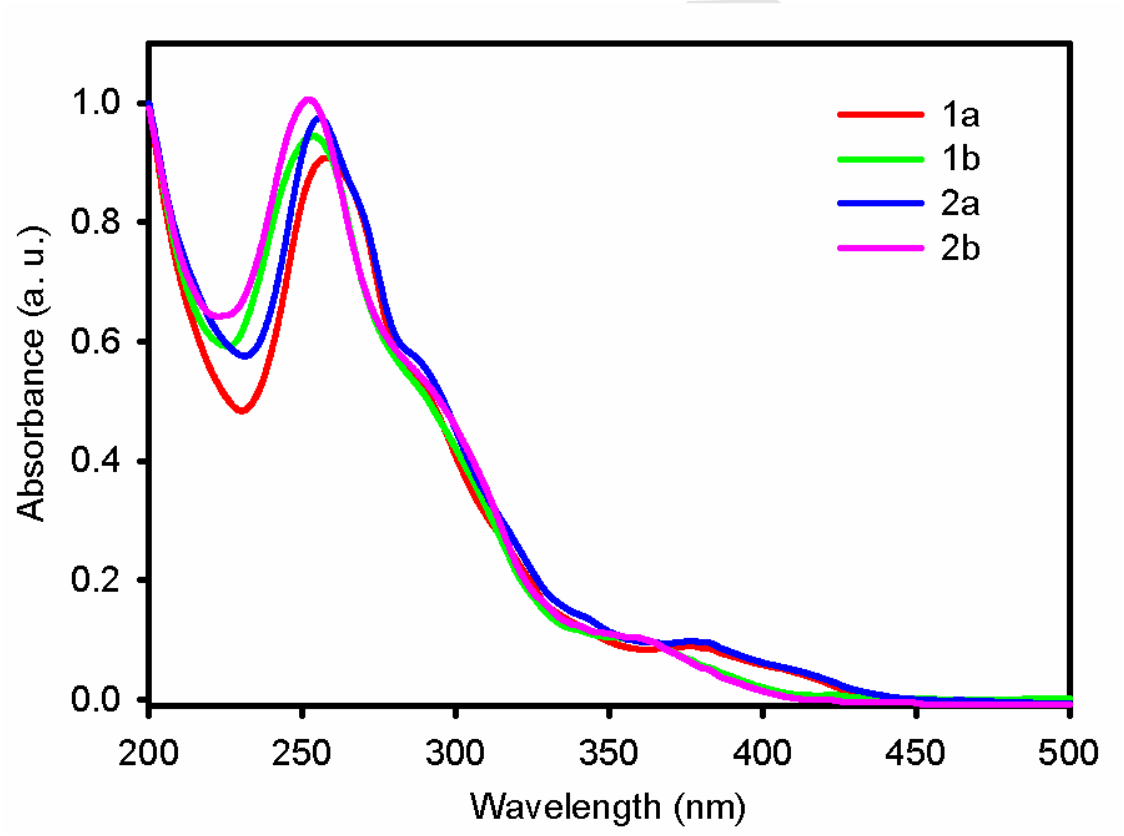

Figure 2. Room temperature UV–visible absorption spectra of cationic iridium complexes (**1a–2b**) in acetonitrile solution.

Table 1. Photophysical and electrochemical properties of cationic iridium complexes **1a**-**2b**.

Complex	λ_{abs}[a] [nm] (ε [× 10^4 M^{-1} cm^{-1}])	Emission at room temperature λ_{em} [nm] Solution[b]	Φ_{em}[c] Solution	Electrochemical data[d] E_{ox} [V]	E_{red} [V]	E_{gap} [eV]
1a	258 (4.23), 287 (2.53), 381 (0.42)	478, 505 sh	0.06	1.39	-1.79	3.18
1b	253 (4.60), 285 (2.62), 363 (0.49)	454, 482 sh	0.10	1.77	-1.73	3.50
2a	255 (5.64), 288 (3.33), 382 (0.55)	476, 504 sh	0.12	1.39	-1.82	3.21
2b	252 (4.34), 290 (2.30), 361 (0.44)	454, 483 sh	0.16	1.72	-1.74	3.46

[a] Absorbance and molar extension coefficients measured in 1.0 × 10^{-5} M acetonitrile solution. [b] Maximum emission wavelength, measured in acetonitrile solution at 1.0 × 10^{-5} M; sh denotes the shoulder wavelength. [c] PL quantum yield of complexes in acetonitrile solution measured versus quinine bisulfate in 1N H_2SO_4. [d] Electrochemical data versus Fc^+/Fc (Fc is ferrocene) measured in 1.0 × 10^{-3} M acetonitrile solution

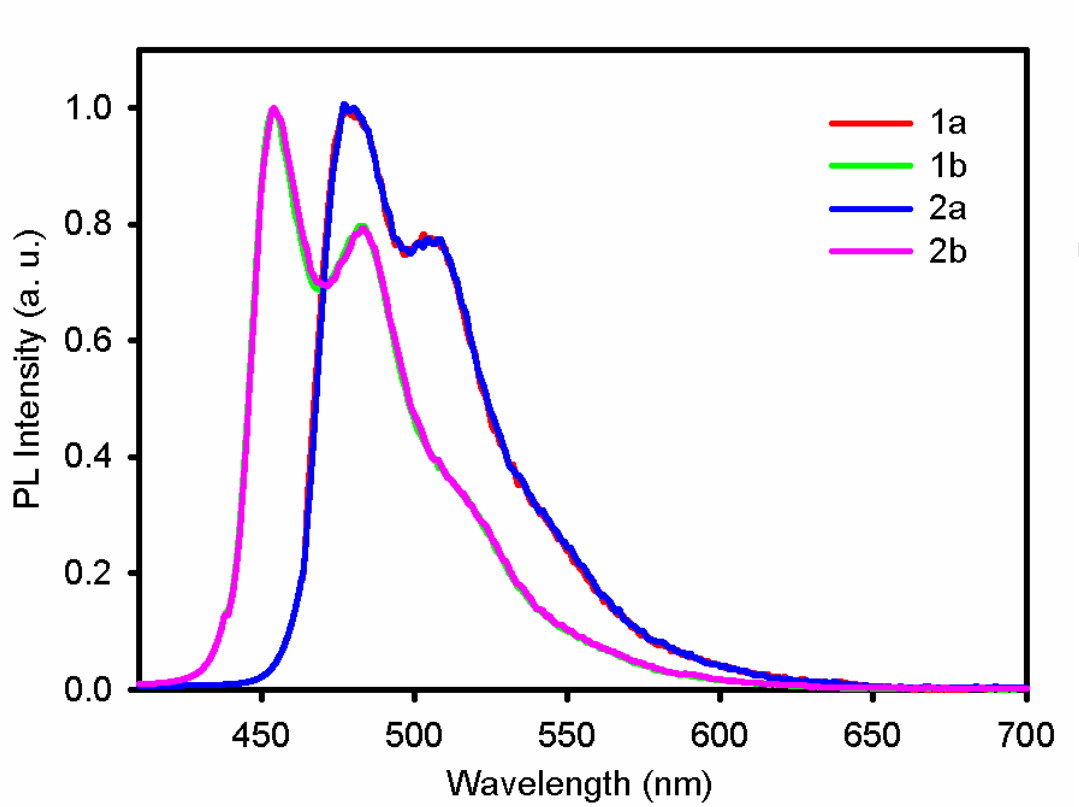

Figure 3. The room temperature photoluminescence (PL) emission spectra of cationic iridium complexes in acetonitrile solutions.

Figure 3 shows the PL emission spectra of the complexes in acetonitrile solution, which were taken at room temperature. The complexes in solution show vibronically structured emission spectra for all the complexes **1a–2b**, indicating that the emissive excited states have a mainly LC $^3\pi$–π^* character and less of a ^{3}MLCT character [34, 36, 37]. In acetonitrile solution, complexes **1a** and **2a** show similar emission properties; complex **1a** has an emission peak at 478 nm and a shoulder peak at 505 nm, whereas those of complex **2a** appear at 476 and 504 nm, respectively. Note that the replacement of the ancillary ligand mepzpy (complex **1a**) with dmpzpy (complex **2a**) does not significantly disturb the photophysical properties of the complexes. However, the emission spectra of complexes **1b** and **2b** display a marked shift toward blue wavelengths relative to those of complexes **1a** and **2a**; **1b** has an emission peak in the blue region at 454 nm

and a shoulder peak at 482 nm, whereas those of **2b** appear at 454 and 483 nm, respectively. The hypsochromic shift in the emission spectra of complexes **1b** and **2b** can be explained by the electron-withdrawing nature of fluorine atoms attached to the cylcometalating ligands, which lowers the energy levels of the complexes by stabilizing the highest occupied molecular orbital (HOMO). The PL quantum yields (PLQYs) of the complexes measured in acetonitrile solution are 0.06, 0.10, 0.12, and 0.16 for complexes **1a**, **1b**, **2a**, and **2b**, respectively. Interestingly, the quantum yields of complexes **2a** and **2b** are higher than those of **1a** and **1b**; this could be due to the additional methyl groups present on the former complexes, which may reduce the intermolecular interactions and excited state self-quenching. The photophysical properties of complexes **1a–2b** are summarized in **Table 1**.

2.3. Electrochemical Properties

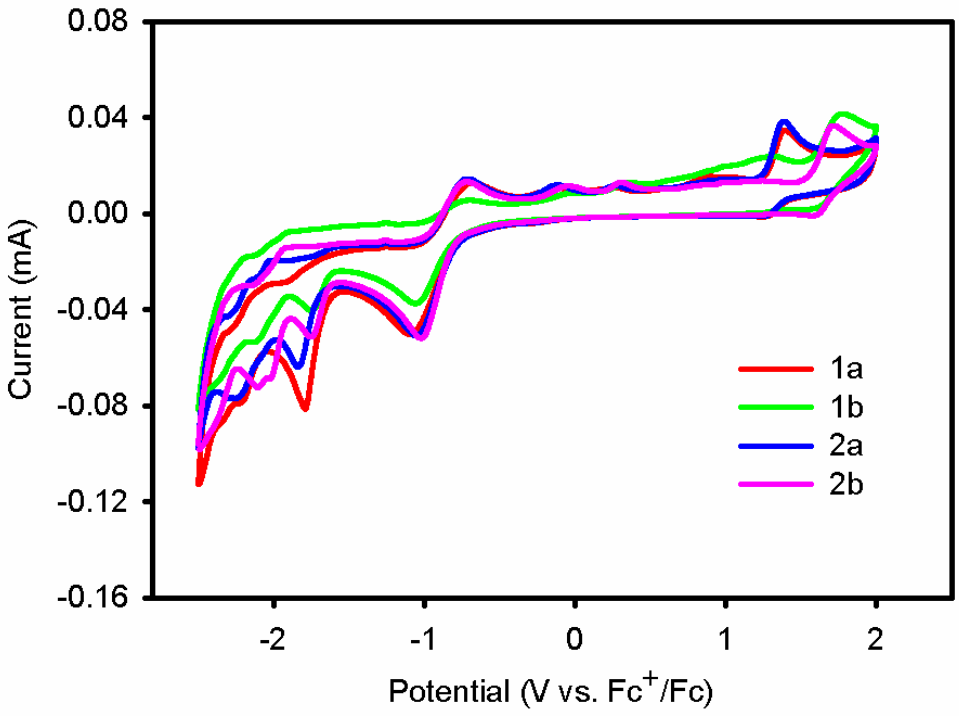

Figure 4. Cyclic voltammograms of complexes (**1a-2b**). The potentials were recorded versus Fc^+/Fc (ferrocenium/ferrocene).

The electrochemical properties of complexes **1a–2b** were investigated by cyclic voltammetry (CV), and the cyclic voltammograms are displayed in **Figure 4**. The redox potentials were measured versus ferrocenium/ferrocene (Fc^+/Fc) using 0.1 M solution of tetrabutylammonium hexafluorophosphate ($TBAPF_6$) in acetonitrile. The electrochemistry data are summarized in **Table 1**. All the complexes display reversible oxidation and irreversible reduction waves in acetonitrile solution. Complexes **1a–2b** show oxidation waves between 1.39 and 1.77 V, attributed to the redox couple of Ir^{III}/Ir^{IV}, with a considerable contribution from the cyclometalated ligands. Compared to complexes **1a** and **2a**, the oxidation potentials of complexes **1b** and **2b** are significantly anodically shifted by ~380 mV owing to the electron-withdrawing fluorine atoms, which reduce the electron density around the iridium center. Upon the cathodic scan, the complexes show irreversible reduction waves at −1.79, −1.73, −1.82, and −1.74 V for complexes **1a**, **1b**, **2a**, and **2b**, respectively. The reduction waves are attributed to the reduction of the ancillary ligand, with a small contribution from cyclometalating ligands. The reduction potentials of complexes **1b** and **2b** are anodically shifted compared to those of complexes **1a** and **2a** owing to the influence of electron-withdrawing fluorine atoms on the cyclometalating ligands. The HOMO and lowest unoccupied molecular orbital (LUMO) energies of complexes **1a–2b** were calculated from the respective oxidation and reduction potentials using the empirical relations. The HOMO energies calculated for complexes **1a**, **1b**, **2a**, and **2b** are −5.76, −6.14, −5.76, and −6.09 eV, respectively, and the LUMO energies are −2.58, −2.64, −2.55, and −2.39 eV, respectively. The electrochemical energy gaps ($E_{gap} = E_{HOMO} - E_{LUMO}$) of complexes **1a**, **1b**, **2a**, and **2b** are 3.18, 3.50, 3.21, and 3.46 eV, respectively.

2.4. Quantum ChemicalCalculations

DFT and TDDFT studies of transition metal complexes are being increasingly used to rationalize their observed optical and photophysical behavior [38]. DFT/TDDFT calculations were performed for complexes **1a**, **1b**, **2a,** and **2b** to gain insights into their structural, electronic, electrochemical and photophysical properties. All the complexes have a pseudo-octahedral coordination geometry around the iridium center. The optimized geometries of the studied complexes are depicted in **Figures 5** and **S1**, and the important geometrical parameters around the iridium center are given in **Table 2**. The bond lengths between the cyclometalated ligands and Ir are nearly 2.02 Å (Ir-C4/Ir-C5) and 2.08 Å (Ir-N3/Ir-N6). For the ancillary ligands, the corresponding distances are somewhat longer, ranging from 2.225 to 2.246 Å. The Ir-N1/Ir-N2 bond distances were found to be longer in **1a** and shorter in **2b**. The bond angles of the cyclometalated phenylpyridine with Ir,*i.e.*, N3-Ir-C4/C5-Ir-N6, were not changed significantly upon substitution and are approximately 80°. On the other hand, the bond angle of ancillary ligands with Ir,*i.e.*, N1-Ir-N2,was found to be approximately 73°. The reported geometrical parameters (bond lengths and bond angles) in **Table 2** do not vary significantly with the change from complex **1a** to complex **2b**.

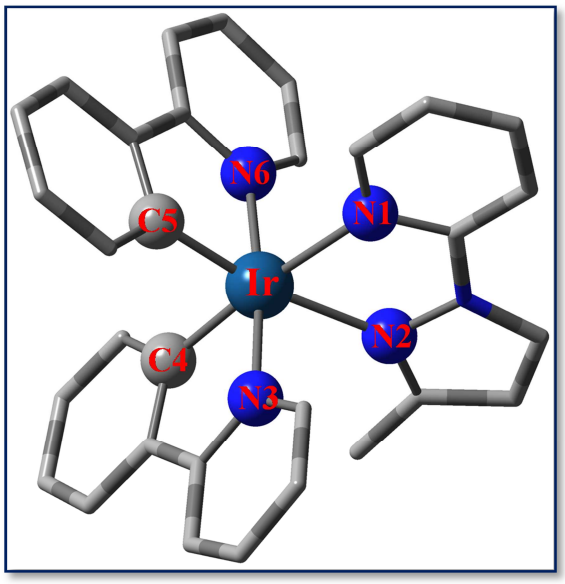

Figure 5. Optimized molecular structure of complex **1a** obtained at the B3LYP/6-31G(d,p)/LanL2DZ level of theory. Hydrogen atoms are omitted for the sake of clarity.

Table 2. Important bond lengths (Å) and bond angles (degrees) of all four metal complexes in their most stable conformations. Atom numbers are shown in **Figure 5**.

	1a	**1b**	**2a**	**2b**
Bond lengths				
Ir-N1	2.240	2.231	2.230	2.225
Ir-N2	2.246	2.233	2.238	2.227
Ir-N3	2.083	2.083	2.083	2.081
Ir-C4	2.021	2.019	2.022	2.020
Ir-C5	2.016	2.015	2.019	2.015
Ir-N6	2.083	2.081	2.080	2.079
Bond angles				
N1-Ir-N2	73.5	73.9	73.1	73.4
N3-Ir-C4	80.1	80.1	80.1	80.1
C5-Ir-N6	80.2	80.3	80.2	80.3

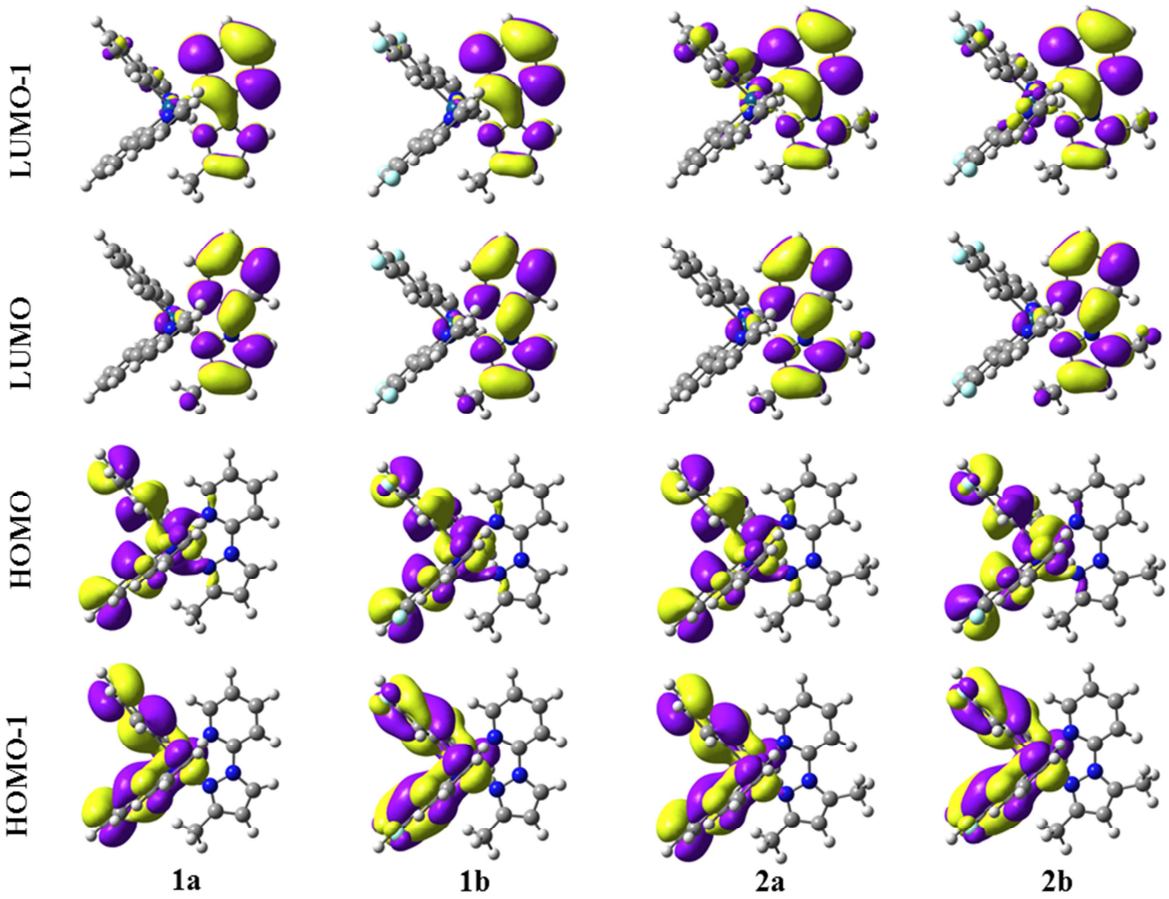

Figure 6. The electron density contours of the HOMO-1 to LUMO+1 of complexes **1a**, **1b**, **2a**, and **2b** (isosurface: 0.02 e $Å^{-3}$) obtained from DFT calculations.

The Kohn–Sham orbitals of the complexes are displayed in **Figure 6**. From the electron density distribution, it is evident that the HOMO and HOMO-1 are generally located on the iridium and the two cyclometalated ligands, whereas the LUMO and LUMO+1 are localized over the ancillary ligand with negligibly small contribution of the Ir orbitals. As the HOMO is centered on the Ir atom and the cyclometalated ligands, any change on these ligands will perturb the HOMO energy to a greater extent compared to the LUMO energy. Therefore, the HOMO is

stabilized by the presence of the electron- withdrawing fluorine atoms on the cyclometalated ligands. The stabilization of the HOMO energy with the change from complex **1a** to **1b** is found to be 0.32 eV, as the energy varying varies from −5.67 eV (complex **1a**) to −5.99 eV (complex **1b**). A similar stabilization of the HOMO energy (0.31 eV) was observed for the change from complex **2a** to **2b**. This stabilization of the HOMO energy by going from complex **1a** to **1b** and also from complex **2a** to **2b** explains the higher oxidation potentials that were experimentally measured for complexes **1b** (1.77 V) and **2b** (1.72 V), compared to those of complexes **1a** (1.39 V) and **2a** (1.39 V). On the other hand, the stabilization of the LUMO energy is insignificant both for the change from complex **1a** to **1b** (0.09 eV) and for the change from complex **2a** to **2b** (0.08 eV). Owing to the unequal stabilization of the HOMO and LUMO energies, the HOMO–LUMO gaps (HLGs) of complexes **1b** (3.32 eV) and **2b** (3.31 eV) are found to be 0.23 eV larger than the corresponding values for **1a** and **2a**. Therefore, considerable hypsochromic shifts in the absorption and emission spectra are expected in the transitions from complex **1a** to **1b** and from complex **2a** to **2b**. The obtained HOMO and LUMO energies and the HLG values from these calculations are in good agreement with the electrochemical data inferred from the CV measurements. The percentage distributions of the HOMO, LUMO, and LUMO+1 are given in Table S1 (complexes **1a** and **1b**) and Table S2 (complexes **2a** and **2b**) for the four Ir complexes In this study, the LUMO level was taken from the sum of the HOMO level and the TDDFT transition energy, rather than from the unreliable Kohn–Sham LUMO eigenvalue [39]. The calculated energy levels of the HOMO and LUMO along with the TDDFT transition energies (Eg) of the four complexes are given in **Table 3**. The HOMO is largely located on the two cyclometalated ligands (~65%) and the Ir (~35%). On the other hand, the reported two lowest

unoccupied orbitals (LUMO and LUMO+1) are centered mainly on the ancillary ligand (~95%), with negligibly small involvement of the Ir and cyclometalated ligands.

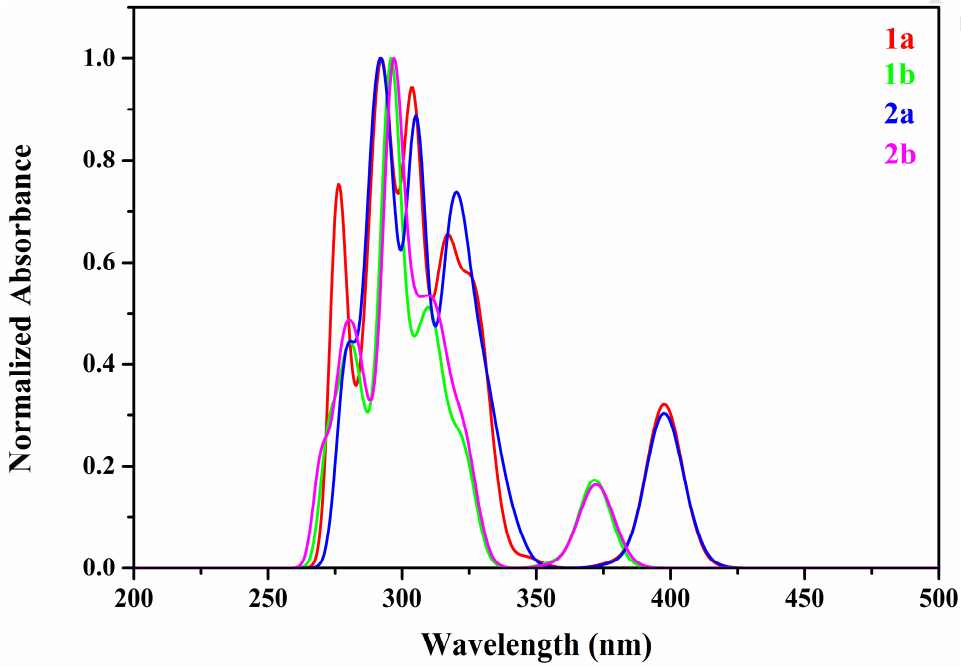

Figure 7. Simulated UV–visible absorption spectra of the four complexes obtained at the B3LYP/6-31G(d,p)/LanL2DZ level of theory. The spectra are broadened using the Gaussian convolution with FWHM=1000 cm^{-1}.

The UV–visible absorption spectra of the four Ir complexes were simulated in acetonitrile solution and are shown in **Figure 7**. The TDDFT simulation reproduced the main bands that were observed in the experimental spectra. The most intense singlet transition in the high wavelength region of complexes **1a** and **2a** is located at 397 nm and those for complexes **1b** and **2b** are located at 371 and 370 nm, respectively. The observed absorption maxima comes from the HOMO → LUMO+1 transition, except for complex **2b**. In complex **2b**, the most intense singlet transition in the high wavelength region mainly arises from the HOMO → LUMO transition. From the percentage contribution (Tables S1 and S2) of the MOs involved in the

transitions, the lowest-lying transitions have mixed MLCT and LLCT character. The observed hypsochromic shift for complexes **1b** and **2b** is attributed to the increased HLG upon fluorine substitution on the cyclometalated ligands (*vide supra*). **Tables 4** and **5** shows the calculated excitation wavelengths with the largest oscillator strengths and coefficients of configuration interaction together with the dominant contribution to each transition. These tables also give the phosphorescence emission data. The TDDFT data show that substitution of the second methyl group on the pyrazole of the ancillary ligand hardly influences the absorption behavior. The simulated UV–visible absorption spectra of the four complexes along with their oscillator strengths are shown in Figure S2.

The phosphorescence emission maxima obtained using the self-consistent field energy difference (ΔSCF) method are 527 and 528 nm for complexes **1a** and **2a**, respectively. Interestingly, the phosphorescence emission maxima of both complexes **1b** and **2b** appear at 502 nm. The calculated emission values are in excellent agreement with the experimental data. We found that both the absorption and emission spectra of complexes **1b** and **2b** are blue-shifted by approximately 26 nm from those of complexes **1a** and **2a**.

Table 3. Calculated energy levels of the frontier molecular orbitals and TDDFT transition energy (E_g) of the four complexes in acetonitrile. All energies are given in eV.

Complex	**1a**	**1b**	**2a**	**2b**
HOMO	-5.67	-5.99	-5.66	-5.97
LUMO	-2.58	-2.67	-2.58	-2.66
E_g, TDDFT ($S_0 \rightarrow S_1$)	3.09	3.32	3.08	3.31

Table 4. Simulated absorption wavelengths (λ_{cal}), oscillator strengths (*f*), and coefficients of configuration interaction (CI) with a dominant contribution to each transition for complexes **1a** and **1b**. The calculated emission values ($\lambda_{emission}$) are obtained using the ΔSCF method. H and L denote HOMO and LUMO, respectively.

Complex	Transitions	λ_{cal} (nm)	f [a]	CI Coefficient	Dominant Contribution	$\lambda_{emission}$ (nm)
1a	$S_0 \rightarrow S_1$	401	0.0146	0.6994	H → L (98%)	527
	$S_0 \rightarrow S_2$	**397**	**0.0985**	**0.6944**	**H → L+1 (96%)**	
	$S_0 \rightarrow S_3$	381	0.0045	0.6966	H → L+2 (97%)	
	$S_0 \rightarrow S_4$	346	0.0075	0.6994	H → L+3 (98%)	
	$S_0 \rightarrow S_5$	332	0.0513	0.4912	H-2 → L (48%)	
	$S_0 \rightarrow T_1$	451		0.5428	H → L+1 (59%)	
	$S_0 \rightarrow T_2$	443		0.4995	H → L+2 (50%)	
	$S_0 \rightarrow T_3$	404		0.6730	H → L (91%)	
	$S_0 \rightarrow T_4$	386		0.3645	H → L+1 (27%)	
	$S_0 \rightarrow T_5$	384		0.4415	H → L+2 (39%)	
1b	$S_0 \rightarrow S_1$	373	0.0318	0.6693	H → L (90%)	502
	$S_0 \rightarrow S_2$	**371**	**0.0755**	**0.6637**	**H → L+1 (88%)**	
	$S_0 \rightarrow S_3$	357	0.0068	0.6921	H → L+2 (96%)	
	$S_0 \rightarrow S_4$	324	0.0807	0.4835	H-1 → L (47%)	
	$S_0 \rightarrow S_5$	323	0.0214	0.5767	H → L+3 (67%)	
	$S_0 \rightarrow T_1$	431		0.4767	H → L+1 (45%)	
	$S_0 \rightarrow T_2$	427		0.4326	H → L+2 (37%)	
	$S_0 \rightarrow T_3$	377		0.6136	H → L (75%)	
	$S_0 \rightarrow T_4$	372		0.2966	H-3 → L (18%)	
	$S_0 \rightarrow T_5$	369		0.4246	H → L+1 (36%)	

[a]The oscillator strengths are given wherever applicable.

Table 5. Simulated absorption wavelengths (λ_{cal}), oscillator strengths (*f*) and coefficients of configuration interaction (CI) with a dominant contribution to each transition for complexes **2a** and **2b**. The calculated emission values ($\lambda_{emission}$) are obtained using the ΔSCF method. H and L denote HOMO and LUMO, respectively.

Complex	Transitions	λ_{cal} (nm)	f [a]	CI Coefficient	Dominant Contribution	$\lambda_{emission}$ (nm)
2a	$S_0 \rightarrow S_1$	402	0.0208	0.6063	H → L (74%)	528
	$S_0 \rightarrow S_2$	**397**	**0.0910**	**0.6023**	**H → L+1 (73%)**	
	$S_0 \rightarrow S_3$	381	0.0034	0.6948	H → L+2 (97%)	
	$S_0 \rightarrow S_4$	341	0.0181	0.6947	H → L+3 (97%)	
	$S_0 \rightarrow S_5$	335	0.0354	0.4970	H-2 → L (49%)	
	$S_0 \rightarrow T_1$	451		0.5646	H → L+1 (64%)	
	$S_0 \rightarrow T_2$	443		0.4994	H → L+2 (50%)	
	$S_0 \rightarrow T_3$	405		0.6816	H → L (93%)	
	$S_0 \rightarrow T_4$	386		0.3752	H → L+1 (28%)	
	$S_0 \rightarrow T_5$	385		0.4281	H → L+2 (37%)	
2b	$S_0 \rightarrow S_1$	375	0.0505	0.5087	H → L+1 (52%)	502
	$S_0 \rightarrow S_2$	**370**	**0.0543**	**0.5121**	**H → L (52%)**	
	$S_0 \rightarrow S_3$	358	0.0045	0.6889	H → L+2 (95%)	
	$S_0 \rightarrow S_4$	325	0.0434	0.4535	H-1 → L (41%)	
	$S_0 \rightarrow S_5$	322	0.0984	0.4927	H-1 → L+1 (49%)	
	$S_0 \rightarrow T_1$	431		0.4949	H → L+1 (49%)	
	$S_0 \rightarrow T_2$	427		0.4317	H → L+2 (37%)	
	$S_0 \rightarrow T_3$	378		0.6279	H → L (79%)	
	$S_0 \rightarrow T_4$	372		0.3693	H-3 → L (27%)	
	$S_0 \rightarrow T_5$	369		0.4126	H → L+1 (34%)	

[a]The oscillator strengths are given wherever applicable.

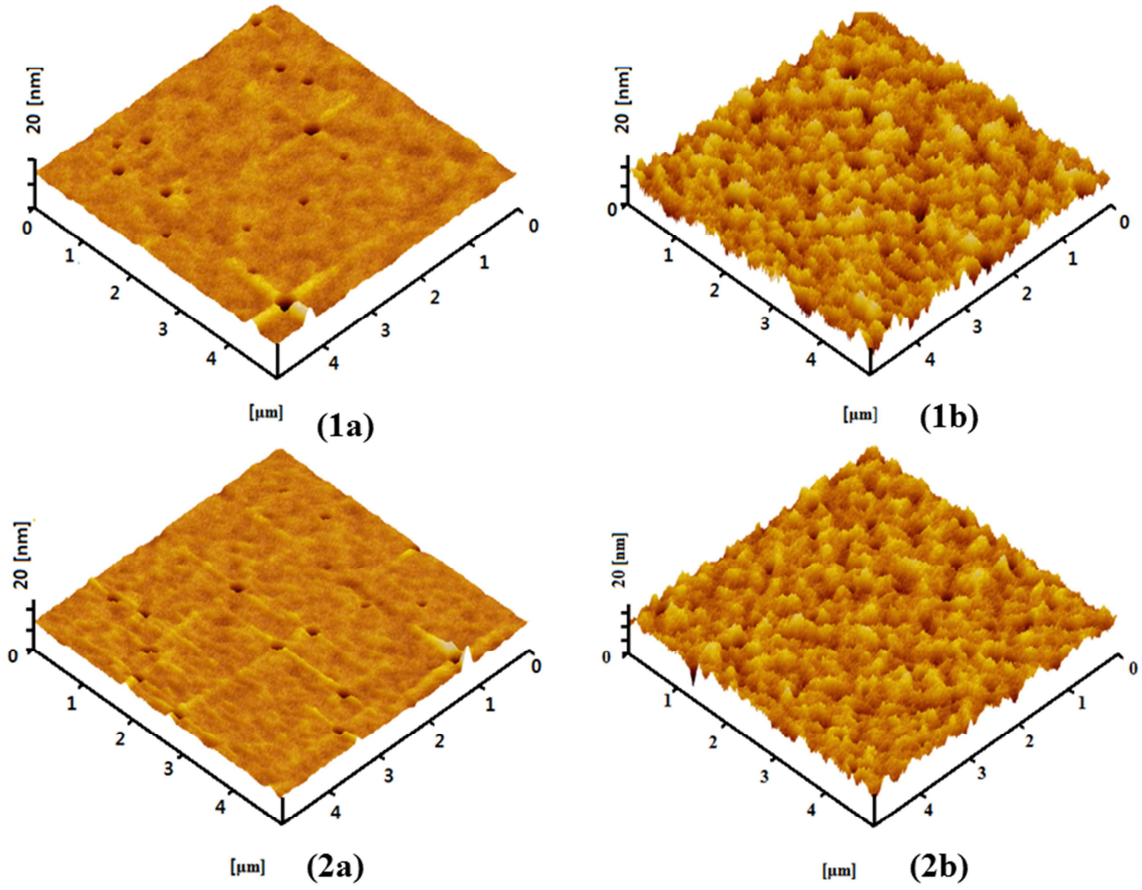

Figure 8. AFM images of thin films of complexes **1a–2b** on top of the ITO/PEDOT:PSS layer.

Electroluminescent properties of LECs

To investigate the electroluminescent properties of complexes **1a–2b**, LECs were fabricated having the device structure of indium tin oxide (ITO)/poly(3,4-ethylenedioxythiophene):polystyrene sulfonate (PEDOT:PSS)/iTMC/Al. The PEDOT:PSS layer was introduced to smooth the ITO surface and facilitate hole injection [37]. To study the thin film surface morphologies of complexes **1a–2b**, atomic force microscopy (AFM) measurements were made, as the film-forming abilities of iTMCs are crucial to better device performance. The films were prepared by spin-coating complexes **1a–2b** on top of the ITO/PEDOT:PSS layer.

Figure 8 shows AFM images of complexes **1a–2b**, which exhibit smooth surface morphology and are pinhole-free. The root-mean-square (rms) roughness values of the neat films of complexes **1b** (0.59 nm) and **2b** (0.51 nm) are lower and hence smoother than **1a** (0.67 nm) and **2a** (0.87 nm). The smaller rms roughness of **2b** indicates that it has excellent film-forming ability.

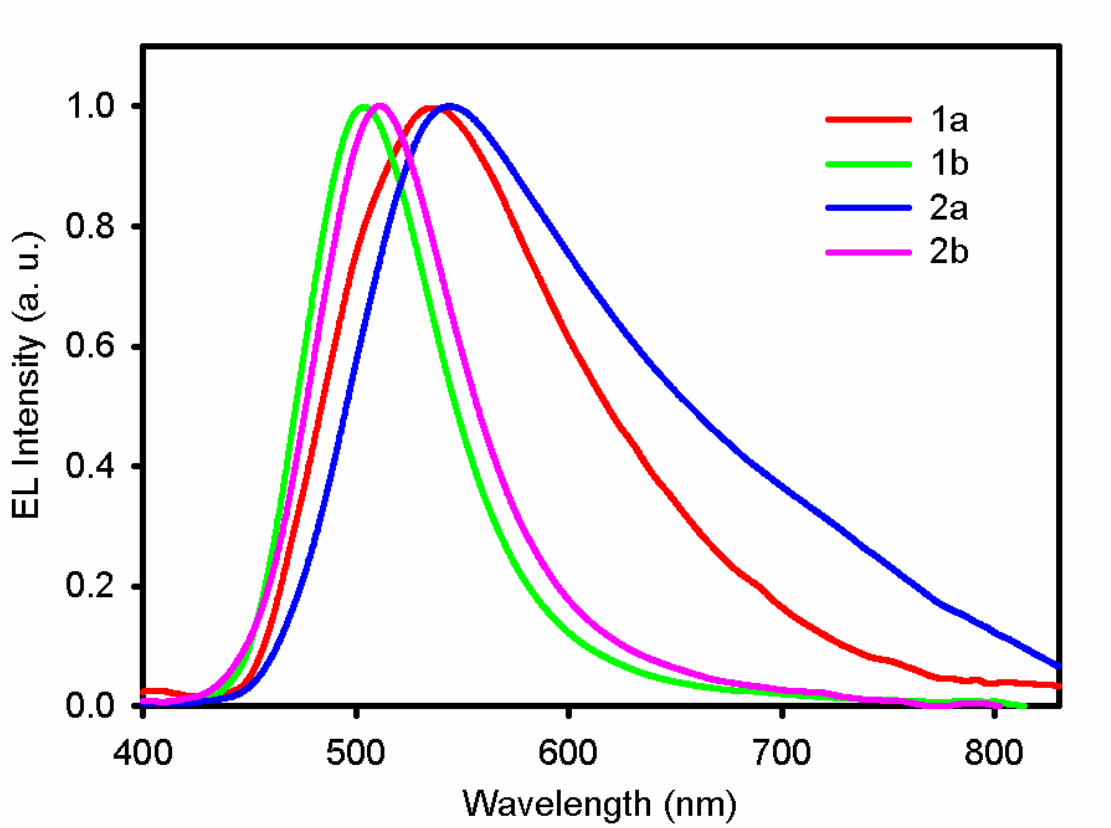

Figure 9. EL spectra of LECs based on cationic iridium complexes **1a–2b**.

The electroluminescence (EL) spectra of the LECs utilizing the cationic iridium complexes **1a–2b** are shown in **Figure 9**. The EL spectra were measured by using a single voltage scan with a sweep rate of 0.5 V/s. Unlike the PL emission spectra in solution, the EL spectra of all the complexes consist of broad, featureless emission peaks, indicating that different optical transitions are responsible for the light emission. The broad emission bands of the EL spectra are

attributed to the existence of stronger intermolecular interaction in the neat film than in the solution. The EL emission maxima of the devices based on **1a** and **1b** are 537 and 503 nm, and those of the devices based on **2a** and **2b** are 543 and 511 nm, respectively. The EL emission of all the complexes is strongly red-shifted compared to the solution PL spectra. This behavior has already been seen in other LEC devices and should be attributed to the polarization effect due to electrical excitation [40, 41]. The Commission Internationale de L'Éclairage (CIE) coordinates of the devices based on complexes **1a** and **2a** are (0.35, 0.51) and (0.34, 0.50), respectively, corresponding to yellow emission. The **1b** device has CIE coordinates of (0.21, 0.51), and those of the **2b** device are (0.24, 0.53), both of which are very close to the green region of the spectrum. The blue shift of the **1b** and **2b** devices is ascribed to the presence of electron-withdrawing substituents on the cyclometalating ligands of both complexes. However, no changes in the band energy and color are observed when we move from complex **1a** to **2a** and **1b** to **2b**, showing that the additional methyl groups on the ancillary ligand do not significantly disturb the energy levels of the complexes.

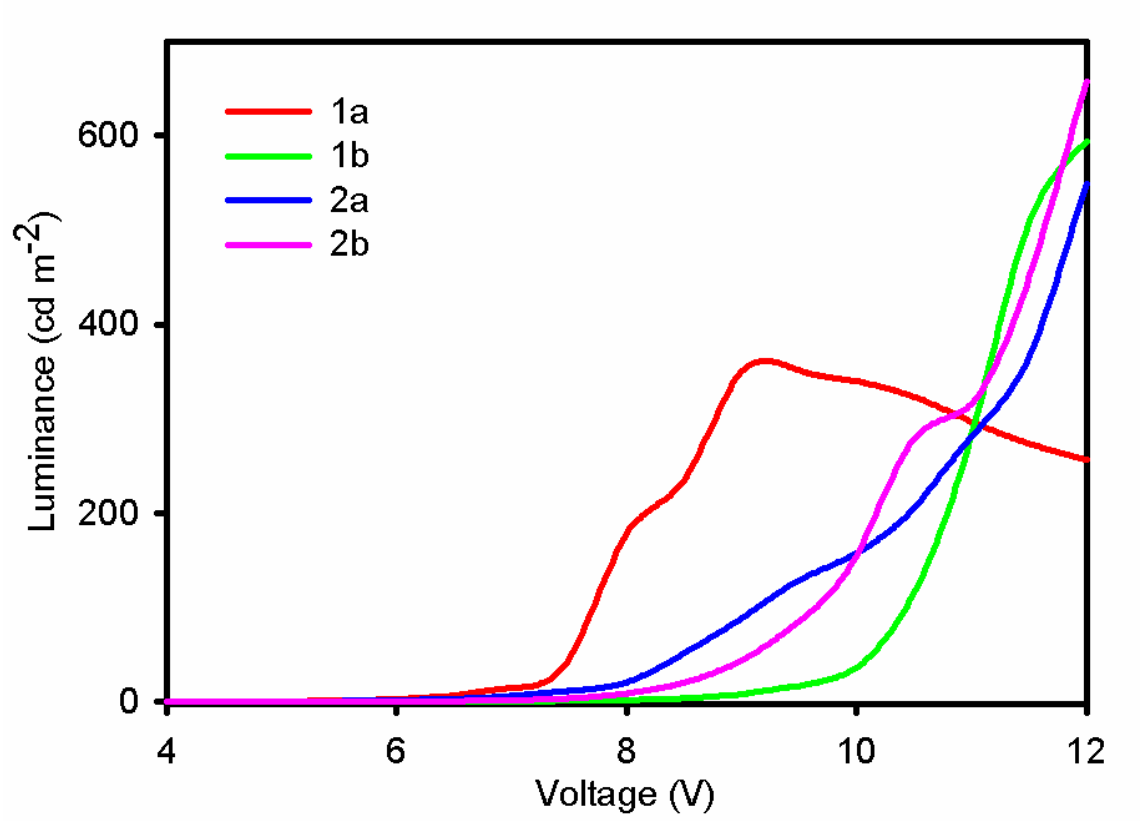

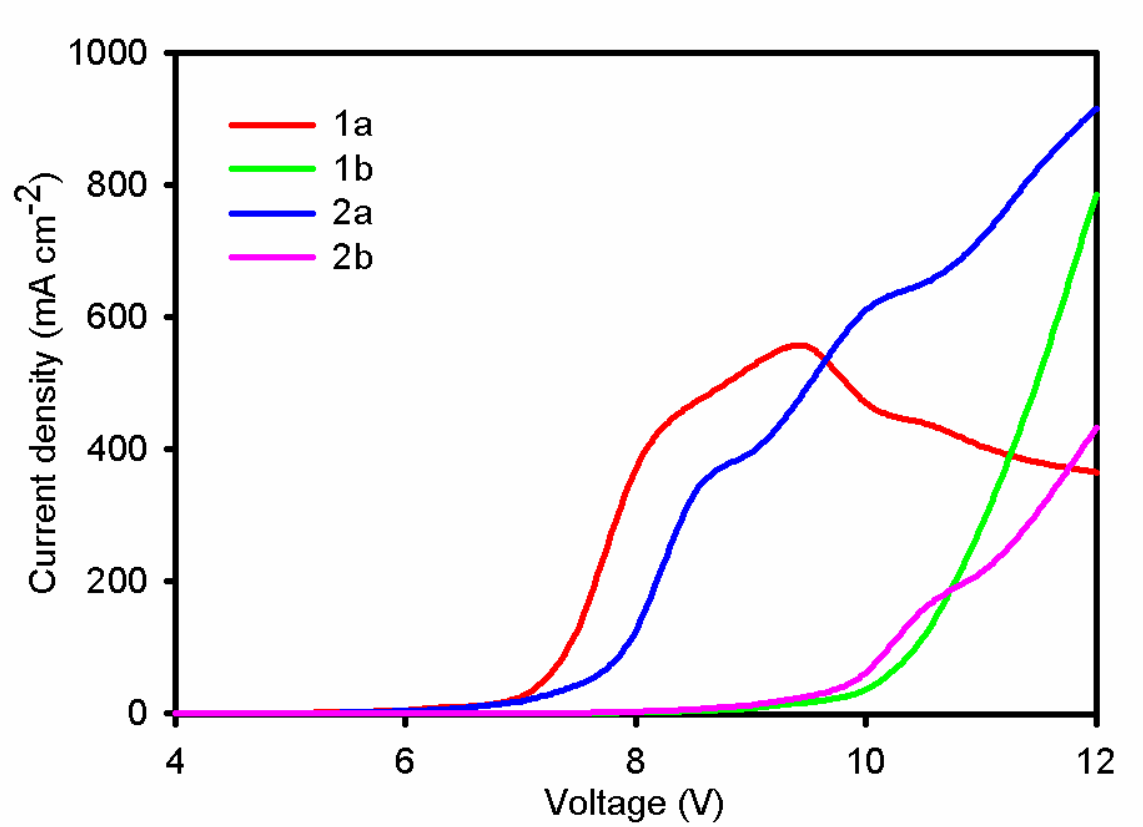

Figure 10. Luminance and current density versus voltage curves of LECs incorporating **1a–2b**.

The luminance and current density versus voltage curves of LECs based on complexes **1a–2b** are shown in **Figure 10**. The luminance and current density of all the devices increase slowly with increasing voltage and reach a maximum intensity, which is a typical characteristic of LEC devices [1, 3]. The delayed response occurring at the starting bias is associated with the slow migration of cations and anions toward the cathode and anode, respectively [3]. The luminance and current density of all the devices are steady up to 8 V and rise sharply with increasing voltage. This is because of rapid ion distribution at the electrode surfaces with increasing voltage, which leads to the creation of a Ir^{IV}/Ir^{III} (p-type) and Ir^{III}/Ir^{II} complexes region (n-type) near the anode and cathode, respectively, followed by an improved carrier injection and recombination. For the device based on **1a**, the luminance and current density increase with

increasing voltage, reaching a maximum value and then decreasing in intensity. The decrease in the intensity of **1a** is associated with low stability of the complexes with increasing voltage or degradation of **1a** during device operation. Compared to **1a**, the device stability of **1b** is higher due to the presence of electron-withdrawing fluorine atoms on cyclometalating ligands, which decrease electron density around iridium center and makes the iridium-cyclometalating ligand bond more stronger. However, on further alkylation, as found in **2a** and **2b**, the ancillary ligands becomes more electron-rich and bind very strongly to the iridium, giving the complexes more stability than **1b** against the attack of water molecules.

Note that the LEC based on **2b** shows the best results, with a maximum luminance of 658 cd m^{-2} and a current efficiency of 0.34 cd A^{-1}. The maximum luminance of the remaining devices follows the order **1b** (560 cd m^{-2}), **2a** (549 cd m^{-2}), and **1a** (351 cd m^{-2}). The peak current efficiencies of the LECs based on **1a**, **1b**, and **2a** are 0.06, 0.31, and 0.07 cd A^{-1}, respectively. The electrical properties of all the LECs are summarized in **Table 6**. The performance of the LEC using **2b** is higher than that of the other device owing to the decreased intermolecular interaction and self-quenching. In addition, the film-forming ability of **2b** yielded a smooth surface and resulted in higher device efficiency than the others. This is because reducing the surface roughness decreases the charge transfer resistance at the interface between the electrodes and the active layer, resulting in more balanced carrier injection and recombination. These results point out that the cationic iridium complexes with smooth surface morphology and the capability of ligands to provide steric hindrance are vital for succeeding efficient, stable devices for solid-state lighting applications.

Table 6. Electrical characteristics of LECs based on **1a-2b.**

Complex	$Luminance_{max}$ [cd m^{-2}]	Current $density_{max}$ [mA cm^{-2}]	Current efficiency (cd A^{-1})	EL_{max} (nm)	CIE coordinates
1a	351	555	0.06	537	(0.35, 0.51)
1b	560	785	0.31	503	(0.21, 0.51)
2a	549	916	0.07	543	(0.34, 0.50)
2b	658	371	0.34	511	(0.24, 0.53)

Experimental Section

Materials and methods

Iridium (III) chloride hydrate, 99.9% ($IrCl_3 \cdot xH_2O$) was purchased from Alfa Aesar, and all the other reactants and solvents were procured from Sigma Aldrich, South Korea, and used without

further purification. ^{1}H and ^{13}C NMR spectra were recorded with a Varian Unity Inova 500 MHz FT-NMR spectrometer. Chemical shifts δ (in ppm) were measured relative to the residual CD_2Cl_2 solvent peak with tetramethylsilane as an internal standard. *J* values are given in Hz. Elemental analyses were carried out with an Elementar Vario EL CHN elemental analyzer. Electrospray ionization mass spectrometry (ESI-MS) analyses were conducted on an Agilent Q-TOF 6530 MS/MS system. Photophysical properties of the complexes were measured at room temperature using 10^{-5} M acetonitrile solution. The UV–visible absorption spectra were recorded in a 1-cm-path-length quartz cell using an Agilent 8453 spectrophotometer. PL emission spectra of the complexes were recorded using an F-7000 FL spectrophotometer. The PLQYs of complexes were measured in solution at an excitation wavelength of 400 nm with quinine bisulfate (Φp = 0.545 in 1 M H_2SO_4) as the reference substance. Oxidation and reduction potentials of the complexes in acetonitrile solution (10^{-3} M) were determined using CV and recorded using a potentiostat/galvanostat (Iviumstat) voltammetric analyzer operated at a scan rate of 100 m V s^{-1}. A glassy carbon and a platinum wire were used as the working and counter electrodes, respectively. The redox potentials of each measurement were recorded versus the Ag/AgCl reference electrode and calibrated with a ferrocenium/ferrocene (Fc^{+}/Fc) couple as an internal standard.The supporting electrolyte was a 0.1 M solution of $TBAPF_6$ in acetonitrile. The HOMO/LUMO energies and energy gaps (E_{gap}) of the complexes were calculated from the oxidation (E_{ox}) and reduction (E_{red}) potentials using the empirical relation[42, 43]: $E_{HOMO} = [-e(E_{ox(vs.\ Ag/AgCl)} - E_{1/2\ (Fc+/Fc\ vs.\ Ag/AgCl))}] - 4.8$ eV, $E_{LUMO} = [-e(E_{red} - E_{1/2})] - 4.8$ eV, and $E_{gap} = E_{HOMO} - E_{LUMO}$, where $E_{1/2\ (Fc+/Fc\ vs.\ Ag/AgCl)}$ is the redox potential of ferrocene (0.43 V), and E_{HOMO} and E_{LUMO} are the energy levels of the HOMO and LUMO, respectively. The surface morphology of the films was studied using AFM (L-Trace II). The films were prepared from

acetonitrile solution by spin-coating the active complexes onto an ITO/PEDOT:PSS layer (see section “Fabrication and Characterization of LECs”).

General synthetic procedure for ancillary ligands (mepzpy and dmpzpy)

The synthesis follows a non-catalyzed C–N coupling reaction in the existence of a potassium *tert*-butoxide base [32].

Synthesis of 2-(3-methyl-1H-pyrazol-1-yl)pyridine (mepzpy). 3-methyl-1H-pyrazole (0.66 g, 8 mmol) and potassium *tert*-butoxide (0.88 g, 7.8 mmol) were dissolved in dry dimethyl sulfoxide (DMSO) (5 mL)at room temperature. To the basic solution, 2-bromopyridine (1.17 g, 7.4 mmol) was added slowly under constant stirring, and the solution was heated to reflux under nitrogen for 12 h. Once the reaction completed, it was cooled to room temperature and extracted with water and ether. The organic layer was washed with water and ether to remove DMSO and excess base. The organic layer was then isolated, dried over anhydrous Na_2SO_4, and filtered. The solvent was then removed under reduced pressure, and the resultant colorless oil was purified by column chromatography on silica gel (200–300 mesh) eluted with hexane/ethylacetate (9:1 v/v). ^{1}H NMR (500 MHz, CD_2Cl_2) δ (ppm): 8.43 (1 H, d, *J*2.53), 8.38 (1 H, d, *J* 4.88), 7.91 (1 H, d, *J* 8.30), 7.79–7.74 (1 H, m), 7.59–7.47 (1 H, m), 6.25 (1 H, d, *J* 2.53), 2.38 (3 H, s).

Synthesis of 2-(3,5-dimethyl-1H-pyrazol-1-yl)pyridine (dmpzpy). The ancillary ligand, dmpzpy, was synthesized in the same manner as mepzpy but using 3,5-dimethyl-1H-pyrazole instead of 3-methyl-1H-pyrazole. A colorless oil was obtained as the product after column chromatography on silica gel eluted with hexane/ethylacetate. ^{1}H NMR (500 MHz, CD_2Cl_2) δ (ppm): 8.40 (1 H, d, *J*2.65), 7.86 (1 H, d, *J*7.86), 7.80–7.71 (1 H, m), 7.60–7.45 (1 H, m), 5.96 (1 H, s), 2.61 (3 H, s), 2.27 (3 H, s).

Synthesis of [Ir(ppy)2(mepzpy)]PF6 (1a). The dichloro-bridged dimeric iridium, $[Ir(ppy)_2Cl]_2$ (108 mg, 0.1 mmol), and mepzpy (37 mg, 0.23 mmol) were dissolved in dichloromethane (15 mL) and methanol (15 mL) and heated to reflux at 60°C under nitrogen for 18 h. After cooling to room temperature, the obtained iridium complex as chloride salts underwent anion metathesis reaction with solid NH_4PF_6 (65 mg, 0.4 mmol). The solvent was then removed under reduced pressure, and the solid obtained was dissolved in dichloromethane to remove insoluble inorganic impurities. The addition of hexane to the filtrate yielded the desired product as a yellow solid, which was then filtered and dried in a vacuum oven for 24 h. The crude material was subsequently crystallized from an acetonitrile/hexane mixture. Yield: 129 mg, 0.16 mmol, 80%. ^{1}H NMR (500 MHz, CD_2Cl_2) δ (ppm): 8.22–8.09 (2 H, m),8.04 (2 H, d, *J*8.74),7.92–7.88 (3 H, m), 7.80–7.74 (3 H, m), 7.64 (1 H, d, *J* 8.30), 7.57 (2 H, d, *J* 4.77), 7.50–7.43 (4 H, m), 7.20–7.16 (2 H, m),6.91–6.80 (2 H, m), 6.20 (1 H, d, *J* 7.64), 1.52 (3 H, s).^{13}C NMR (126 MHz, CD_2Cl_2) δ (ppm): 161.42, 157.13, 150.65, 149.93, 145.10, 142.09, 139.24, 137.13, 135.89, 130.05, 129.38, 128.01, 127.54, 126.10, 124.93, 121.91, 120.12, 113.25, 105.21, 15.61. Anal. Calcd (%) for $C_{31}H_{25}N_5PF_6Ir$: C, 46.27; H, 3.13; N, 8.70. Found: C, 46.21; H, 3.18; N, 8.79. ESI-MS (*m*/*z*): 660.2 $[M\text{-}PF_6]^+$.

Synthesis of $[Ir(dfppy)_2(mepzpy)]PF_6$ (1b). The synthesis was similar to that of 1a but replacing $[Ir(ppy)_2Cl]_2$ with $[Ir(dfppy)_2Cl]_2$. Yield: 136 mg, 0.15 mmol, 78%. ^{1}H NMR (500 MHz, CD_2Cl_2) δ (ppm): 8.36 (2 H, d, *J* 7.50), 8.23–8.14 (4 H, m), 7.85–7.71 (3 H, m), 7.62–7.56 (2 H, m), 7.24 (2 H, s), 7.15 (2 H, s, *J* 6.64), 6.62–6.51 (2 H, m), 6.23 (1 H, d, *J* 7.58), 1.54 (3 H, s). ^{13}C NMR (126 MHz, CD_2Cl_2) δ (ppm): 164.65, 161.98, 160.48, 157.23, 150.90, 150.01, 142.34, 139.27, 137.60, 135.44, 129.73, 127.91, 124.60, 124.05, 112.63, 111.80, 104.11, 99.83,

15.67. Anal. Calcd (%) for $C_{31}H_{21}N_5PF_{10}Ir$: C, 42.47; H, 2.41; N, 7.99. Found: C, 42.50; H, 2.50; N, 8.08. ESI-MS (*m*/*z*): 732.1 $[M\text{-}PF_6]^+$.

Synthesis of $[Ir(ppy)_2(dmpzpy)]PF_6$ (2a). The complex was obtained as a yellow solid by treating $[Ir(ppy)_2Cl]_2$ (108 mg, 0.1 mmol) and dmpzpy (40 mg, 0.23 mmol). Yield: 130 mg, 0.16 mmol, 79%. ^{1}H NMR (500 MHz, CD_2Cl_2) δ (ppm): 8.12–8.09 (2 H, m), 8.03 (2 H, d, *J*8.72), 7.97–7.93 (3 H, m), 7.86 (1 H, d, *J*1.58), 7.84–7.80 (3 H, m), 7.74–7.69 (2 H, m), 7.57 (2 H, d, *J* 5.10), 7.24–7.21 (2 H, m), 7.12–7.04 (3 H, m), 6.27 (1 H, s), 2.88 (3 H, s), 1.68 (3 H, s). ^{13}C NMR (126 MHz, CD_2Cl_2) δ (ppm): 161.27, 156.02, 150.80, 150.19, 149.25, 144.28, 144.03, 141.64, 138.54, 131.13, 130.62, 124.95, 123.86, 120.03, 113.86, 105.36, 15.72, 13.78. Anal. Calcd (%) for $C_{32}H_{27}N_5PF_6Ir$: C, 46.94; H, 3.32; N, 8.55. Found: C, 46.97; H, 3.33; N, 8.62. ESI-MS (*m*/*z*): 674.2 $[M\text{-}PF_6]^+$.

Synthesis of $[Ir(dfppy)_2(dmpzpy)]PF_6$ (2b). This complex was synthesized from $[Ir(dfppy)_2Cl]_2$ (122 mg, 0.1 mmol) and dmpzpy (40 mg, 0.23 mmol). Yield: 144 mg, 0.16 mmol, 81%. ^{1}H NMR (500 MHz, CD_2Cl_2) δ (ppm): 8.33 (2 H, d, *J* 8.75), 8.19–8.15 (2 H, m), 8.08 (1 H, d, *J*8.66), 7.81–7.77 (3 H, m), 7.58 (1 H, d, *J* 5.84), 7.31–7.28 (2 H, m),7.17–7.12 (3 H, m), 6.62–6.51 (2 H, m), 6.31 (1 H, s), 2.91 (3 H, s), 1.76 (3 H, s). ^{13}C NMR (126 MHz, CD_2Cl_2) δ (ppm): 164.70, 162.76, 160.69, 156.22, 152.72, 151.88, 149.38, 146.17, 142.42, 139.69, 128.17, 124.66, 124.05, 112.85, 111.33, 104.32, 99.07, 15.68, 13.83. Anal. Calcd (%) for $C_{32}H_{23}N_5PF_{10}Ir$: C, 43.15; H, 2.60; N, 7.86. Found: C, 43.19; H, 2.65; N, 7.82. ESI-MS (*m*/*z*): 746.2 $[M\text{-}PF_6]^+$.

Quantum chemical calculations

All the DFT and TDDFT simulations for the four cationic iridium (III) complexes were conducted using the Gaussian 09 (Revision B.01) *ab initio* quantum chemical program [44].

Geometry optimization and vibrational frequency analysis of the complexes were performed by employing a hybrid Becke [45, 46] three-parameter Lee–Yang–Parr [47] exchange-correlation functional (B3LYP). We used 6-31G(d,p) basis functions for the H, C, N, and F atoms. We used a "double-ξ" quality basis set consisting of Hay and Wadt's effective core potentials (LanL2DZ ECP) [48-50] for the Ir atom. No symmetry constraints were applied during geometry optimization. Vibrational frequency analysis was conducted to confirm that each configuration is indeed a local minimum on the potential energy surface. The contour plots for the molecular orbitals were generated using the GaussView program [51].

On the basis of the optimized structures of the electronic ground state (S_0), the UV–visible absorption spectra of the four Ir complexes were obtained using the TDDFT formalism in acetonitrile solution to mimic the experimental conditions. The phosphorescence emission data were obtained by employing the ΔSCF method. The absorption and emission properties of the complexes in acetonitrile solvent were calculated in association with the polarizable continuum model [52, 53] implemented in Gaussian G09. The TDDFT calculations were performed using the B3LYP functional and the mixed basis set as described above. This level of theory has been shown to give reliable results for the structural, electronic, and optical properties of transition metal complexes [54].

Fabrication and characterization of LECs

ITO-coated glass plates patterned by conventional photolithography were purchased from Samsung Corning, South Korea. These glass substrates were cleaned by sonication in a mixture of solvents consisting of acetone, ethanol, and isopropyl alcohol (1:1 v/v) for 30 min. After being dried, the ITO substrates underwent UV–ozone treatment for 30 min. PEDOT:PSS was purchased from H. C. Starck (Clevios AI 4083). Before spin-coating, the PEDOT:PSS solution

was filtered using a 0.2 μm hydrophilic polytetrafluoroethylene (PTFE) filter. The hole-conducting PEDOT:PSS layer was used to improve the reproducibility of the devices and to avoid the formation of pinholes.

The iTMC-LECs were fabricated as follows. First, the PEDOT:PSS solution was spin-coated onto the precleaned ITO substrate at 2000 rpm for 20 s. The spin-coated films were then baked at 120°C for 10 minin a vacuum oven. Next, the active layer solution was spin-coated onto the ITO/PEDOT:PSS layer and baked at 70°C for 1 h. The active layer solution was prepared from 20 $mgmL^{-1}$ acetonitrile solution. Before spin-coating, the active layer solution was kept in a shaking incubator for 24 h and then filtered by a 0.1 μm hydrophobic PTFE filter. The substrate containing the spin-coated active layer was then subjected to thermal evaporation to deposit the aluminum cathode (100 nm)in a metal-evaporating chamber using a shadow mask under high vacuum. The consequential devices had the structure of ITO/PEDOT:PSS/iTMC/Al. The electrical properties of these devices were evaluated in ambient conditions using Keithley characterization systems. The voltage dependent current density and luminance of the devices were measured using a Keithley 2400 source meter with a sweep rate of 0.5 V s^{-1} and were calibrated with a silicon photodiode. An Avantes luminance spectrometer was used to measure the EL spectrum and CIE coordinates.

Conclusions

We reported the synthesis and photophysical and electrochemical characterization of four new cationic iridium complexes with methyl-substituted pyrazole ligands, namely, $[Ir(ppy)_2(mepzpy)]PF_6$ (**1a**), $[Ir(dfppy)_2(mepzpy)]PF_6$ (**1b**), $[Ir(ppy)_2(dmpzpy)]PF_6$ (**2a**), and $[Ir(dfppy)_2(dmpzpy)]PF_6$ (**2b**), for solid-state light-emitting applications. The complexes were

synthesized in good yields; complexes **1a** and **2a** exhibited blue-green emission in acetonitrile solution, and **1b** and **2b** exhibited blue emission. The additional methyl groups present in **2a** do not produce any significant change in the photophysical properties; however, the change in the substituents on the cyclometalating ligands could tune the emission properties of the complexes. DFT and TDDFT calculations were performed for all the complexes, and the results were consistent with the observed photophysical and electrochemical properties. LECs were fabricated; their emission was red-shifted compared to the PL spectra in acetonitrile solution, resulting in yellow emission for complexes **1a** and **2a** and green emission for complexes **1b** and **2b**. Moreover, a higher luminance of 658 cd m^{-2} and current efficiency of 0.34 cd A^{-1} were obtained for the LEC based on **2b** owing to the reduced intermolecular interactions as well as a smooth surface morphology. This work demonstrates that steric hindrance on metal complexes is essential for improved device performance, as it suppresses self-quenching and inhibits the nonradiative pathways. In addition, the film-forming abilities of the iridium complexes are also crucial for enhanced device performance.

ASSOCIATED CONTENT

Supporting Information

"This information is available free of charge via the Internet at http://pubs.acs.org/."

AUTHOR INFORMATION

*Corresponding author: *choe@pusan.ac.kr*

* Corresponding author. Tel.: +8251 510 2396; Fax: +8251 512 8634

E-mail address: choe@pusan.ac.kr

Notes

The authors declare no competing financial interest.

Acknowledgement

This research was financially supported by the "2015 Post-Doc. Development Program of Pusan National Universsity, South Korea".

References

[1] Pei Q, Yu G, Zhang C, Yang Y, Heeger AJ. Polymer Light-Emitting Electrochemical Cells. Science. 1995;269(5227):1086-8.
[2] Lowry MS, Hudson WR, Pascal RA, Bernhard S. Accelerated Luminophore Discovery through Combinatorial Synthesis. Journal of the American Chemical Society. 2004;126(43):14129-35.
[3] Slinker JD, Gorodetsky AA, Lowry MS, Wang J, Parker S, Rohl R, et al. Efficient Yellow Electroluminescence from a Single Layer of a Cyclometalated Iridium Complex. Journal of the American Chemical Society. 2004;126(9):2763-7.
[4] Slinker JD, DeFranco JA, Jaquith MJ, Silveira WR, Zhong Y-W, Moran-Mirabal JM, et al. Direct measurement of the electric-field distribution in a light-emitting electrochemical cell. Nat Mater. 2007;6(11):894-9.
[5] Sunesh CD, Shanmugasundaram K, Subeesh MS, Chitumalla RK, Jang J, Choe Y. Blue and Blue-Green Light-Emitting Cationic Iridium Complexes: Synthesis, Characterization, and Optoelectronic Properties. ACS Applied Materials & Interfaces. 2015;7(14):7741-51.
[6] Lee JK, Yoo DS, Handy ES, Rubner MF. Thin film light emitting devices from an electroluminescent ruthenium complex. Applied Physics Letters. 1996;69(12):1686-8.
[7] Gao FG, Bard AJ. Solid-State Organic Light-Emitting Diodes Based on Tris(2,2'-bipyridine)ruthenium(II) Complexes. Journal of the American Chemical Society. 2000;122(30):7426-7.
[8] Rudmann H, Rubner MF. Single layer light-emitting devices with high efficiency and long lifetime based on tris(2,2[′] bipyridyl) ruthenium(II) hexafluorophosphate. Journal of Applied Physics. 2001;90(9):4338-45.
[9] Hosseini AR, Koh CY, Slinker JD, Flores-Torres S, Abruña HD, Malliaras GG. Addition of a Phosphorescent Dopant in Electroluminescent Devices from Ionic Transition Metal Complexes. Chemistry of Materials. 2005;17(24):6114-6.
[10] Wang Y-M, Teng F, Hou Y-B, Xu Z, Wang Y-S, Fu W-F. Copper(I) complex employed in organic light-emitting electrochemical cells: Device and spectra shift. Applied Physics Letters. 2005;87(23):-.

[11] Kalsani V, Schmittel M, Listorti A, Accorsi G, Armaroli N. Novel Phenanthroline Ligands and Their Kinetically Locked Copper(I) Complexes with Unexpected Photophysical Properties. Inorganic Chemistry. 2006;45(5):2061-7.
[12] Sunesh CD, Sunseong O, Chandran M, Moon D, Choe Y. Effect of ionic liquids on the electroluminescence of yellowish-green light-emitting electrochemical cells using bis(2-(2,4-difluorophenyl)pyridine)4,7-diphenyl-1,10-phenanthroline-iridium(III) hexafluorophosphate. Materials Chemistry and Physics. 2012;136(1):173-8.
[13] Sunesh CD, Chandran M, Mathai G, Choe Y. Highly luminescent yellow and yellowish-green light-emitting electrochemical cells based on cationic iridium complexes with phenanthroline based ancillary ligands. Optical Materials. 2013;35(3):407-13.
[14] Sunesh CD, Chandran M, Ok S, Choe Y. Effect of Smaller Counter Anion, BF4 –, on the Electroluminescent Properties of Cationic Iridium Complex Based Light-Emitting Electrochemical Cells. Molecular Crystals and Liquid Crystals. 2013;584(1):131-8.
[15] Bernhard S, Gao X, Malliaras GG, Abruña HD. Efficient Electroluminescent Devices Based on a Chelated Osmium(II) Complex. Advanced Materials. 2002;14(6):433-6.
[16] Zhang Q, Zhou Q, Cheng Y, Wang L, Ma D, Jing X, et al. Highly Efficient Electroluminescence from Green-Light-Emitting Electrochemical Cells Based on CuI Complexes. Advanced Functional Materials. 2006;16(9):1203-8.
[17] Slinker J, Bernards D, Houston PL, Abruna HD, Bernhard S, Malliaras GG. Solid-state electroluminescent devices based on transition metal complexes. Chemical Communications. 2003(19):2392-9.
[18] Bernhard S, Barron JA, Houston PL, Abruña HD, Ruglovksy JL, Gao X, et al. Electroluminescence in Ruthenium(II) Complexes. Journal of the American Chemical Society. 2002;124(45):13624-8.
[19] Buda M, Kalyuzhny G, Bard AJ. Thin-Film Solid-State Electroluminescent Devices Based On Tris(2,2‘-bipyridine)ruthenium(II) Complexes. Journal of the American Chemical Society. 2002;124(21):6090-8.
[20] Felici M, Contreras-Carballada P, Smits JMM, Nolte RJM, Williams RM, De Cola L, et al. Cationic Heteroleptic Cyclometalated IridiumIII Complexes Containing Phenyl-Triazole and Triazole-Pyridine Clicked Ligands. Molecules. 2010;15(3):2039-59.
[21] Costa RD, Ortí E, Bolink HJ, Monti F, Accorsi G, Armaroli N. Luminescent Ionic Transition-Metal Complexes for Light-Emitting Electrochemical Cells. Angewandte Chemie International Edition. 2012;51(33):8178-211.
[22] Hu T, He L, Duan L, Qiu Y. Solid-state light-emitting electrochemical cells based on ionic iridium(iii) complexes. Journal of Materials Chemistry. 2012;22(10):4206-15.
[23] Sunesh CD, Mathai G, Choe Y. Green and blue–green light-emitting electrochemical cells based on cationic iridium complexes with 2-(4-ethyl-2-pyridyl)-1H-imidazole ancillary ligand. Organic Electronics. 2014;15(3):667-74.
[24] Sunesh CD, Choe Y. Synthesis and characterization of cationic iridium complexes for the fabrication of green and yellow light-emitting devices. Materials Chemistry and Physics. 2015;156(0):206-13.
[25] Sunesh CD, Ok S, Mathai G, Choe Y. Electroluminescent properties of yellow light-emitting electrochemical cells based on a cationic iridium complex and the effect of ionic liquids incorporation in an active layer. Thin Solid Films. 2013;531(0):530-4.

[26] Sunesh CD, Mathai G, Cho Y-R, Choe Y. Optoelectronic properties of green and yellow light-emitting electrochemical cells based on cationic iridium complexes. Polyhedron. 2013;57(0):77-82.
[27] Costa RD, Ortí E, Bolink HJ, Graber S, Housecroft CE, Constable EC. Intramolecular π-Stacking in a Phenylpyrazole-Based Iridium Complex and Its Use in Light-Emitting Electrochemical Cells. Journal of the American Chemical Society. 2010;132(17):5978-80.
[28] Graber S, Doyle K, Neuburger M, Housecroft CE, Constable EC, Costa RD, et al. A Supramolecularly-Caged Ionic Iridium(III) Complex Yielding Bright and Very Stable Solid-State Light-Emitting Electrochemical Cells. Journal of the American Chemical Society. 2008;130(45):14944-5.
[29] Su HC, Fang FC, Hwu TY, Hsieh HH, Chen HF, Lee GH, et al. Highly Efficient Orange and Green Solid-State Light-Emitting Electrochemical Cells Based on Cationic IrIII Complexes with Enhanced Steric Hindrance. Advanced Functional Materials. 2007;17(6):1019-27.
[30] He L, Duan L, Qiao J, Dong G, Wang L, Qiu Y. Highly Efficient Blue-Green and White Light-Emitting Electrochemical Cells Based on a Cationic Iridium Complex with a Bulky Side Group. Chemistry of Materials. 2010;22(11):3535-42.
[31] Sunesh CD, Mathai G, Choe Y. Constructive Effects of Long Alkyl Chains on the Electroluminescent Properties of Cationic Iridium Complex-Based Light-Emitting Electrochemical Cells. ACS Applied Materials & Interfaces. 2014;6(20):17416-25.
[32] Shavaleev NM, Scopelliti R, Baranoff E, Grätzel M, Nazeeruddin MK. Charged cyclometalated iridium(III) complexes that have large electrochemical gap. Inorganica Chimica Acta. 2012;383(0):316-9.
[33] Nonoyama M. Benzo[<I>h</I>]quinolin-10-yl-<I>N</I> Iridium(III) Complexes. Bulletin of the Chemical Society of Japan. 1974;47(3):767-8.
[34] Sprouse S, King KA, Spellane PJ, Watts RJ. Photophysical effects of metal-carbon .sigma. bonds in ortho-metalated complexes of iridium(III) and rhodium(III). Journal of the American Chemical Society. 1984;106(22):6647-53.
[35] Lamansky S, Djurovich P, Murphy D, Abdel-Razzaq F, Lee H-E, Adachi C, et al. Highly Phosphorescent Bis-Cyclometalated Iridium Complexes: Synthesis, Photophysical Characterization, and Use in Organic Light Emitting Diodes. Journal of the American Chemical Society. 2001;123(18):4304-12.
[36] Colombo MG, Brunold TC, Riedener T, Guedel HU, Fortsch M, Buergi H-B. Facial tris cyclometalated rhodium(3+) and iridium(3+) complexes: their synthesis, structure, and optical spectroscopic properties. Inorganic Chemistry. 1994;33(3):545-50.
[37] Tamayo AB, Garon S, Sajoto T, Djurovich PI, Tsyba IM, Bau R, et al. Cationic Bis-cyclometalated Iridium(III) Diimine Complexes and Their Use in Efficient Blue, Green, and Red Electroluminescent Devices. Inorganic Chemistry. 2005;44(24):8723-32.
[38] Di Censo D, Fantacci S, De Angelis F, Klein C, Evans N, Kalyanasundaram K, et al. Synthesis, Characterization, and DFT/TD-DFT Calculations of Highly Phosphorescent Blue Light-Emitting Anionic Iridium Complexes. Inorg Chem. 2008;47(3):980-9.
[39] Zhang G, Musgrave CB. Comparison of DFT Methods for Molecular Orbital Eigenvalue Calculations. The Journal of Physical Chemistry A. 2007;111(8):1554-61.
[40] Bolink HJ, Cappelli L, Cheylan S, Coronado E, Costa RD, Lardies N, et al. Origin of the large spectral shift in electroluminescence in a blue light emitting cationic iridium(iii) complex. Journal of Materials Chemistry. 2007;17(48):5032-41.

[41] Dreyse P, Loeb B, Soto-Arriaza M, Tordera D, Orti E, Serrano-Perez JJ, et al. Effect of free rotation in polypyridinic ligands of Ru(ii) complexes applied in light-emitting electrochemical cells. Dalton Transactions. 2013;42(43):15502-13.
[42] Liu Y, Liu MS, Jen AKY. Synthesis and characterization of a novel and highly efficient light-emitting polymer. Acta Polymerica. 1999;50(2-3):105-8.
[43] Hwang S-W, Chen Y. Synthesis and Electrochemical and Optical Properties of Novel Poly(aryl ether)s with Isolated Carbazole and p-Quaterphenyl Chromophores. Macromolecules. 2001;34(9):2981-6.
[44] Frisch MJ, Trucks GW, Schlegel HB, Scuseria GE, Robb MA, Cheeseman JR, et al. Gaussian 09, Revision B.01. Wallingford CT2009.
[45] Becke AD. Density-functional thermochemistry. III. The role of exact exchange. The Journal of Chemical Physics. 1993;98(7):5648-52.
[46] Becke AD. Density-functional thermochemistry. IV. A new dynamical correlation functional and implications for exact-exchange mixing. The Journal of Chemical Physics. 1996;104(3):1040-6.
[47] Lee C, Yang W, Parr RG. Development of the Colle-Salvetti correlation-energy formula into a functional of the electron density. Physical Review B. 1988;37(2):785-9.
[48] Hay PJ, Wadt WR. Ab initio effective core potentials for molecular calculations. Potentials for the transition metal atoms Sc to Hg. The Journal of Chemical Physics. 1985;82(1):270-83.
[49] Hay PJ, Wadt WR. Ab initio effective core potentials for molecular calculations. Potentials for K to Au including the outermost core orbitals. The Journal of Chemical Physics. 1985;82(1):299-310.
[50] Wadt WR, Hay PJ. Ab initio effective core potentials for molecular calculations. Potentials for main group elements Na to Bi. The Journal of Chemical Physics. 1985;82(1):284-98.
[51] GaussView, Version 5, Roy Dennington, Todd Keith, John Milliam, Semichem Inc., Shawnee Mission KS, 2009.
[52] Miertuš S, Scrocco E, Tomasi J. Electrostatic interaction of a solute with a continuum. A direct utilizaion of AB initio molecular potentials for the prevision of solvent effects. Chemical Physics. 1981;55(1):117-29.
[53] Cossi M, Barone V, Cammi R, Tomasi J. Ab initio study of solvated molecules: a new implementation of the polarizable continuum model. Chemical Physics Letters. 1996;255(4–6):327-35.
[54] Chitumalla RK, Gupta KSV, Malapaka C, Fallahpour R, Islam A, Han L, et al. Thiocyanate-free cyclometalated ruthenium(ii) sensitizers for DSSC: A combined experimental and theoretical investigation. Physical Chemistry Chemical Physics. 2014;16(6):2630-40.

Highlights

- Iridium complexes (1a-2b) were synthesized using pyrazole based ancillary ligands.
- DFT and TDDFT calculations were performed for all complexes
- Light-emitting electrochemical cells (LECs) were fabricated and characterized.
- LECs based on these complexes resulted in yellow and green electroluminescence.